Simulation and Experimental Demonstration of a Tolerant and Low-loss III-V-to-Si$_3$N$_4$ Adiabatic Coupling Structure

Biwei Pan
Photonics Research Group, INTEC,
Ghent University - imec
Ghent, Belgium
biwei.pan@UGent.be

Pim Voorthuijzen
SMART Photonics,
Eindhoven, The Netherlands
pim.voorthuijzen@smartphotonics.nl

Diego Carbajal Altamirano
IMEC,
Leuven, Belgium
diego.carbajal@imec.be

Cian Cummins
IMEC,
Leuven, Belgium
cian.cummins@imec.be

Sandeep Seema Saseendran
IMEC,
Leuven, Belgium
Sandeep.SeemaSaseendran@imec.be

Philippe Helin
IMEC,
Leuven, Belgium
philippe.helin@imec.be

Marcus Dahlem
IMEC,
Leuven, Belgium
marcus.dahlem@imec.be

Jing Zhang
Photonics Research Group, INTEC,
Ghent University - imec
Ghent, Belgium
jingzhan.zhang@ugent.be

Gunther Roelkens
Photonics Research Group, INTEC,
Ghent University - imec
Ghent, Belgium
gunther.roelkens@UGent.be

Abstract—A fabrication-tolerant and low-loss III-V-to-Si$_3$N$_4$ adiabatic coupling structure is designed and experimentally demonstrated. The simulation shows an excess loss less than -0.3-dB at +/-1-um lateral misalignment with the DVS-BCB bonding layer thickness varying from 10 to 70 nm. A micro-transfer printed III-V-to-Si$_3$N$_4$ coupler was measured to have a ~ -0.7 dB loss per coupler over a 1510 nm to 1610 nm wavelength range.

Keywords—heterogeneous integration, optical interconnection, photonic integrated circuits

I. Introduction

Silicon photonics is becoming a highly competitive technology that offers promising solutions in various fields such as chip-to-chip communication, quantum computing and LiDAR. Leveraging the advanced and mature CMOS manufacturing, silicon (Si) and silicon nitride (Si$_3$N$_4$) photonics provides a reliable and low-cost integration platform that contains multiple functions such as passive devices, modulators and photodetectors. However, limited by their indirect bandgap, on-chip light sources and amplifiers have to rely on III-V materials, where efficient optical coupling between Si/Si$_3$N$_4$ and III-V waveguides is essential.

Vertical couplers serve as a key component to enable III-V-to-Si/Si$_3$N$_4$ coupling in heterogeneous integration, like die/wafer-to-wafer bonding [1] and micro-transfer printing [2]. Depending on the behavior of optical modes in the coupling structure, there are two kinds of vertical couplers, resonant couplers and adiabatic couplers. The adiabatic couplers maintain optical power in the fundamental mode during power transfer through slowly changing of the waveguide geometry, which shows better fabrication and lateral misalignment tolerant [3]. This advantage is crucial for high-throughput wafer-level heterogeneous integration.

In this paper, we present a III-V-to-Si$_3$N$_4$ adiabatic vertical coupler with high-fabrication-tolerance of both lateral misalignment and DVS-BCB bonding layer thickness. A measurement structure was proposed to experimentally test its coupling loss and a micro-transfer printed III-V-to-Si$_3$N$_4$ coupler was measured.

II. Vertical Coupler Design

In order to realize vertical coupling between III-V and Si$_3$N$_4$, a two stage III-V-to-Si-to-Si$_3$N$_4$ structure is used to overcome the large refractive index mismatch between them. Taking advantage of simple manufacturing, a hydrogenated amorphous silicon (aSi:H) interlayer is adopted to replace crystalline silicon as the interlayer [4]. Since the aSi:H-to-Si$_3$N$_4$ coupler is typically fabricated in a silicon photonics foundry with high-precision lithography, a linear taper can provide tolerances within the fabrication capability. Here, we focused on the design of the III-V-to-aSi:H coupler, which would be implemented through heterogeneous integration, where the misalignment tolerance is crucial. The detailed design and fabrication tolerance analysis of the III-V-to-aSi:H coupler are discussed below.
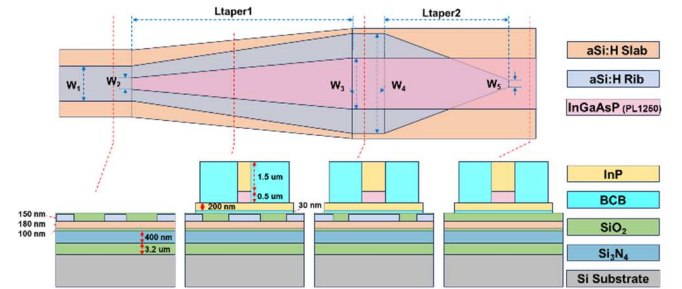

Fig. 1. Schematic diagram of the proposed III-V-to-aSi:H vertical coupler

Figure 1 shows a schematic diagram of the proposed III-V-to-aSi:H coupling structure and its cross sections at different locations along the coupler. It consists of two parts of waveguide tapers, where the left part (L$_{taper1}$) partially couples the optical power from aSi:H to III-V by linearly increasing the waveguide widths of both waveguides. Through further tapering down the aSi:H waveguide in the right part (L$_{taper2}$), the remaining optical power in the aSi:H would be fully transmit to the III-V waveguide. W$_1$-W$_5$ are defined as the widths of the aSi:H and III-V waveguides at relevant positions as shown in the schematic. W$_2$ and W$_5$ are set as 0.4 μm and 0.18 μm, respectively, corresponding to the

minimum feature size defined in the process design kit. W_3 and W_4 are fixed as 2 and 5.5 μm. Although linear tapers are used here for the coupling, this concept can be easily transferred to multisegmented structures [5]. Ansys Lumerical EME solver is used to optimize the designs and analyze the fabrication tolerances. The refractive index of aSi:H, SiO_2 and Si_3N_4 was measured by ellipsometry and the refractive indexes of InP and InGaAsP (photoluminescence = 1250 nm) were calculated using the Tanguy model with parameters given in [6]. Figure 2(a) shows the simulated coupling efficiencies versus the lengths of L_{taper1} at different lateral misalignments, where W_1 and L_{taper2} are set as 3.5 um and 100
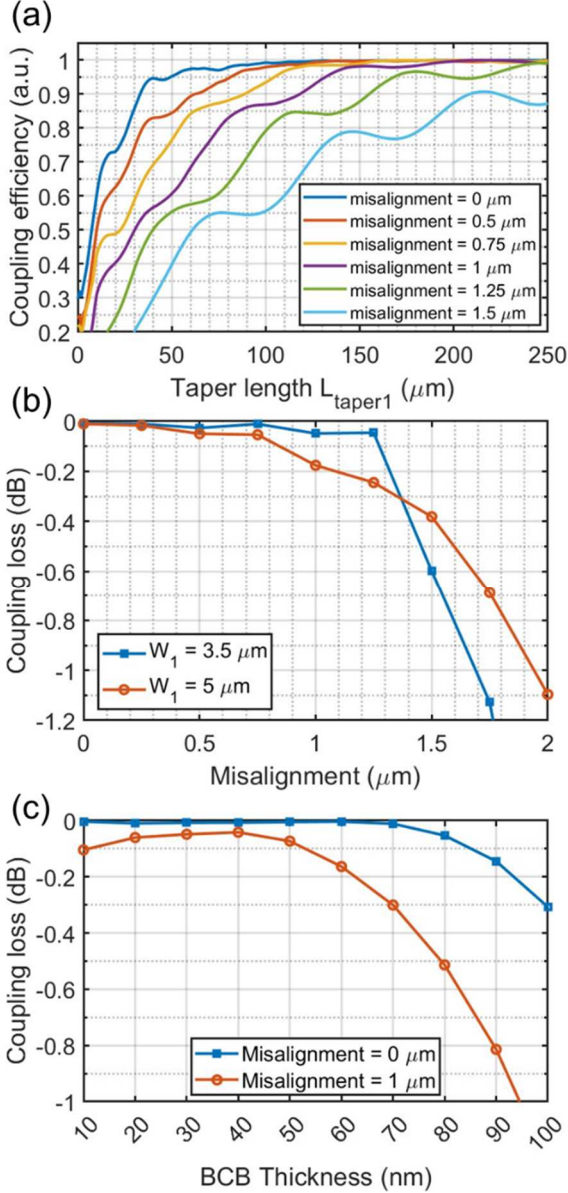
Fig. 2. (a) Simulated coupling efficiency versus the length of left taper (L_{taper1}) under different lateral misalignments; (b) Simulated coupling loss versus the lateral misalignment under different width of W_1; (c) Simulated coupling loss as a function of BCB thicknesses under different misalignments.

um, respectively. As can be seen, when L_{taper1} is 250 um, a 1-μm misalignment can be tolerated with 99% coupling efficiency. Fig. 2(b) shows the coupling loss as a function of misalignment for different widths of W_1. It can be seen that when the misalignment is less than 1.25 μm, the narrower

aSi:H waveguide can provide better power coupling due to less coupling to high-order modes. In the case of larger lateral misalignment, the mode decoupling between the two waveguides would be more severe for narrower W_1, which leads to a rapid increase of the coupling loss. A less than -0.2-dB extra loss is expected at +/-1-um lateral misalignment for different widths of W_1, which also represents high misalignment tolerance along the transmission direction. The simulated thickness tolerance of the DVS-BCB bonding layer is shown in Figure 2(c), where the coupling loss stays less than -0.3 dB with the thickness varying from 10 to 70 nm when there is 1-μm lateral misalignment or varying from 0 to 100 nm when there is no misalignment.

III. COUPLING LOSS MEASUREMENT

In order to measure the coupling loss, an array of structures with different numbers of vertical couplers was designed and fabricated. A microscope picture of the proposed structure and a zoom-in view are shown in Figure 3(b) and (c), respectively, where III-V coupons based on materials from SMART photonics are integrated on the aSi:H/Si_3N_4 circuits through micro-transfer printing. The schematic diagram of the measurement setup is shown in Figure 3(a). The optical power (0 dBm) from a tunable laser (Santec TSL-510) is coupled into the chip through a grating coupler on the Si_3N_4 layer probed by a cleaved standard single-mode fiber. The spectrum of each device is collected using an optical power meter (HF 81532A), while scanning the laser's wavelength. In each measurement, the polarization state of the input signal is carefully adjusted to achieve maximum transmission power.
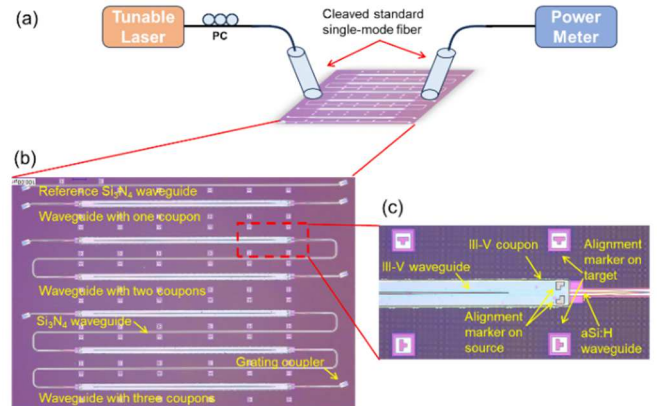

Fig. 3. (a) Schematic diagram of the measurement setup (PC: polarization contoller); (b) Microscope picture of the fabricated coupling loss measurement structure; (c) Zoom-in view of micro-transfer printed III-V coupon on an aSi:H/Si_3N_4 circuit.

Figure 4(a) shows the transmission spectra of the test structures. The transmission loss of the reference waveguide arises from the fiber coupling loss and parabolic wavelength dependence of the input and output grating couplers. We can detect some periodic fluctuations from the spectra that contain III-V coupons, which would result from the beating of excited higher-order modes during the evanescent coupling when there is lateral misalignment. It can be seen from the spectra that the fluctuation amplitude is relatively small, which corresponds to a weak excitation of high-order modes.

Figure 4(b) shows the coupling losses extracted from the subtraction between the transmission of one or two coupons and the reference waveguide. As can be seen, the loss per coupler is ~ -0.7dB in a wavelength range of 1510 nm to 1610 nm. The extracted coupling loss contains III-V waveguide loss

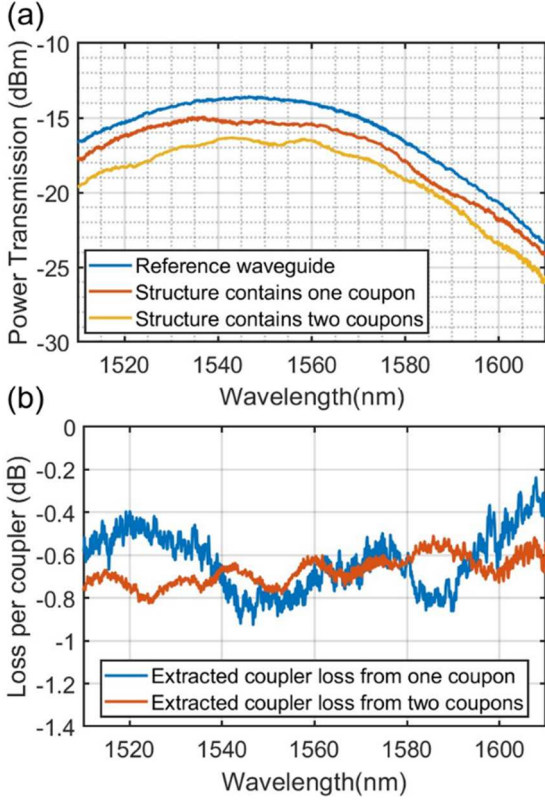that has half of the coupon length (500 um), which would overestimate the coupling loss by about 0.1 dB.

Fig. 4.   (a) Measured transmission spectra of the test structures; (b) Spectra of the extracted coupling loss.

IV. CONCLUSION

We demonstrated a high-fabrication-tolerant and low-loss III-V-to-Si_3N_4 adiabatic vertical coupling structure. The design shows high tolerance for both lateral misalignment and DVS-BCB bonding layer thickness. The coupling loss of a micro-transfer printed III-V-to-Si_3N_4 coupler was experimentally measured, where a ~ -0.7 dB loss per coupler is realized in a wavelength range of 1510 nm to 1610 nm. The proposed vertical coupler is expected to find its application in high-throughput heterogenous integration.

REFERENCES

[1]   Y. Wan, C. Xiang, J. Guo, R. Koscica, MJ Kennedy, J. Selvidge,Z. Zhang, L. Chang, W. Xie, D. Huang, A. C. Gossard, and J. E. Bower, "High Speed Evanescent Quantum-Dot Lasers on Si," Laser Photonics Rev, vol. 15, August 2021, p. 2100057.

[2]   G. Roelkens, J. Zhang, L. Bogaert, M. Billet, D. Wang, B. Pan, C. J. Kruckel, E. Soltanian, D. Maes, T. Vanackere, T. Vandekerckhove, S. Cuyvers, J. De Witte, I. L. Lufungula, X. Guo, H. Li, S. Qin, G. Muliuk, S. Uvin, B. Haq, C. Op de Beeck, J. Goyvaerts, G. Lepage, P. Verheyen, J. Van Campenhout, G. Morthier, B. Kuyken, D. Van Thourhout, R. Baets, "Micro-Transfer Printing for Heterogeneous Si Photonic Integrated Circuits," IEEE Journal of Selected Topics in Quantum Electronics, vol. 29, no. 3, May-June, pp. 1-14.

[3]   X. Sun, H. Liu, and A. Yariv, "Adiabaticity criterion and the shortest adiabatic mode transformer in a coupled-waveguide system," Opt. Lett. vol. 34, February 2009, pp. 280-282.

[4]   C. O. d. Beeck, B. Haq, L. Elsinger, A. Gocalinska, E. Pelucchi, B. Corbett, G. Roelkens, and B. Kuyken, "Heterogeneous III-V on silicon nitride amplifiers and lasers via microtransfer printing," Optica, vol. 7, no. 5, May 2020, pp. 386-393.

[5]   C. Yao, Q. Cheng, G. Roelkens, and R. Penty, "Bridging the gap between resonance and adiabaticity: a compact and highly tolerant vertical coupling structure," Photon. Res. vol. 10, September 2022, pp. 2081-2090.

[6]   S. Seifert and P. Runge, "Revised refractive index and absorption of In1-xGaxAsyP1-y lattice-matched to InP in transparent and absorption IR-region," Opt. Mater. Express, vol. 6, January 2016, pp. 629-639.

PROGRAM OVERVIEW

📢 **Click here** to submit your post-deadline paper.

Sunday 30 June 2024   Monday 1 July 2024   Tuesday 2 July 2024   Wednesday 3 July 2024

Thursday 4 July 2024

Thursday 4 July 2024

13:45 - 14:00	Monitoring Based on Modified Godard Algorithm for Short-reach Coherent Optics *Mr Jianwei Tang*		200Gbaud 32QAM Single-Carrier Signal on Thin-Film Lithium Niobate Platform *Dr Yixiao Zhu*		slope-efficiency O Modulator and Am Reception *Dr Paikun Zhu*
14:00 - 14:15	**#221 -** Polarization Demultiplexing Aided by an Optical Domain SOP Tracking Prototype *Miss Wanxin Zhao*	**#101 -** 100Gbps PAM4 operation of EML sub-assembly by using novel glass sub-mount *Mr Takuma Fujita*	**#476 -** First Demonstration of Pre-Amplified 200G Self-Coherent PON *Dr Haojie Zhu*	**#192 -** Analogue of electromagnetically induced absorption in the microwave domain based on a reflective-type microring resonator *A/Prof Zhenzhou Tang*	**#37 -** Improvemen OFDM Transmissi Chirp Silicon MRM *Prof Leslie Rusch*
14:15 - 14:30	**#176 -** High accuracy and robustness RSOP monitoring based on machine learning *Miss Shuning Sun*	**#129 -** Wavelength-sweeping VCSEL as the light source for fiber optic gyroscope *Ms Yu-Tong Lee*	**#462 -** Wavelength- temporal-interleaved Microwave Photonic Signal Processer on Silicon *Miss Qingrui Yao*	**#160 -** 200-krad/s Polarization Tracking Using Thin Film Lithium Niobate Integrated Dynamic Polarization Controller *Mr Youxin Liu*	**#22 -** Real-Time 4 Transmission Ena Injection-Locked D Modulated Laser *Dr Gleb Nazarikov*
14:30 - 14:45	**#122 -** Joint estimation of OSNR and Shaping Distribution for PCS signals using amplitude histogram *Mr Shunta Muto*	**#284 -** 1550-nm-Band Quantum Dot Distributed Bragg Reflector Laser Using Intermixing Monolithic Integration *Dr Atsushi Matsumoto*	**#465 -** Distributed Vibration Sensing Using a 3 MHz linewidth DFB laser over 55.9 km of Weakly-Coupled Multicore Fibe Enabled by Balanced Delay Line Laser Interferometry *Mr Yaguang Hao*	**#137 -** Simulation and Experimental Demonstration of a Tolerant and Low-loss III-V-to-Si3N4 Adiabatic Coupling Structure *Biwei Pan*	**#203 -** Real-Time Measurement Usin Sideband Modulat Zehnder Modulato *Mr Qingchuan Hua*
14:45 - 15:00	**#105 -** Ultra-simple Chromatic Dispersion Estimation Utilizing RF Pilot Tone Power Evolution for Coherent Systems	**#395 -** 200 GHz Grid QD Colliding Pulse Mode-locked Laser for High-speed	**#466 -** GPS-stabilized Optical Frequency Combs for Freqency-synchrous Optical Networks	**#133 -** Layer-dependent nonlinear optical absorption in 2D layered MXene films for hybrid integrated photonics	**#76 -** Stokes Vecto Direct Detection S Enabling Polarizat Rotation Without T